A deep marine organic carbon reservoir in the non-glacial Cryogenian ocean (Nanhua Basin, South China) revealed by organic carbon isotopes

Xi Peng[1, 2], Xiang-Kun Zhu[1, *], Fuqiang Shi[1], Bin Yan [1], Feifei Zhang [1], Nina Zhao [1], Pingan Peng[2], Jin Li [1], Graham A. Shields[3]

1. MLR Key Laboratory of Isotope Geology, Institute of Geology, Chinese Academy of Geological Sciences, Beijing 100037, China
2. State Key Laboratory of Organic Geochemistry, Guangzhou Institute of Geochemistry, Chinese Academy of Sciences, Guangzhou 510640, China
3. Department of Earth Sciences, University College London, Gower Street, London, WC1E 6BT, UK

*Corresponding author. Tel.: +86 1068999798

E-mail address: xiangkun@cags.ac.cn

Abstract

The late-Cryogenian warm (non-glacial) interval or LCWI (c.660 – c.650 Ma) is potentially of great significance to the co-evolution between life and the surface environment during the emergence of animal life on Earth. Although oxygenation has been frequently used to explain the timing of animal evolution and diversification, few studies have focused on the net source of oxygen, sedimentary

organic carbon, during this interval. In this study, three high-resolution organic carbon isotopic ($\delta^{13}C_{org}$) records for the Datangpo Formation (=Xiangmeng Formation) on the Yangtze platform are presented. The data derive from drill cores representing different depositional settings at Daotuo (slope), Minle (shallower-basin), and Xiangtan (deep-basin), respectively. The Daotuo and Minle samples exhibit an overall increase of 6-8‰ as well as significant isotopic fluctuations following the Tiesi'ao (=Sturtian) glaciation, while samples from the deeper Xiangtan section show relatively muted fluctuations (±1‰) and no overall trend over the same interval. These findings can potentially be explained by a much longer residence time for marine organic matter, which may have acted as a redox buffer against oxygenation and climate change. The build-up and eventual oxidation of a sub-pycnocline organic carbon reservoir in the redox stratified non-glacial ocean could help to explain the extreme positive and negative carbon isotope excursions, respectively, in time-equivalent shallow-marine carbonate platform successions from Mongolia, Australia and Namibia.

Keywords: Cryogenian non-glacial interval, Nanhua Basin, organic carbon isotopes, organic carbon reservoir, oxygenation

1 Introduction

The Neoproterozoic Era is of great significance in the evolutionary history of the

Earth system and life. A series of important geological events occurred during this era, known widely by their evocative nicknames: 'Snowball Earth'; the 'Neoproterozoic Oxygenation Event'; and the 'Cambrian Explosion' (Holland, 1999, 2006; Squire et al., 2006; Canfield et al, 2007; Frei et al, 2009; Campbell and Squire, 2010; Halverson and Shields-Zhou, 2011; Smith et al., 2013; Lyons et al., 2014; Zhang et al., 2014; Chen et al., 2015; Sperling et al., 2015). Accompanying these various upheavals was a series of extremely negative excursions in the carbon isotopic composition of marine carbonates ($\delta^{13}C_{carb}$), the origin of which is hotly debated (Halverson et al., 2002; Grotzinger et al., 2011; Kump et al., 2011; Johnston et al., 2012; Rose et al., 2012; Schrag et al., 2013; Fan et al., 2014). Suggested causes of the negative excursions (by as much as 10‰ to 15‰) are: diagenetic alteration; decreased primary productivity; methane-seepage; petroleum-seepage; and repeated oxidation of a large 'dissolved' organic carbon reservoir due to pulsed oxygenation (Halverson et al., 2002; Fike et al., 2006; McFadden et al., 2008; Swanson-Hysell et al., 2010; Jiang, et al., 2012; Johnston et al., 2012; Lee et al, 2015), or deep seawater upwelling (Fan et al., 2014).

Rothman et al. (2003) proposed the existence of a large dissolved organic carbon (DOC) reservoir to explain the extreme carbon isotope fluctuations of the Neoproterozoic Era (Rothman et al., 2003), and this model has received further support since (Fike et al., 2006; McFadden et al., 2008; Swanson-Hysell et al., 2010; Kump et al., 2011). Much of the emphasis in these later studies has been to examine the relationship between $\delta^{13}C_{carb}$ excursions and the carbon isotopic composition of

organic carbon ($\delta^{13}C_{org}$), and in particular whether the two show the same trends or are decoupled from each other. If $\delta^{13}C_{carb}$ and $\delta^{13}C_{org}$ are coupled, it is suggested that they both formed from the same dissolved inorganic carbon (DIC) reservoir (Johnston et al., 2012). If $\delta^{13}C_{carb}$ and $\delta^{13}C_{org}$ are decoupled, they are both subordinate to the DOC reservoir (McFadden et al., 2008; Swanson-Hysell et al., 2010). A two-component mixing model was used by Johnston et al. (2012) to argue that apparent decoupling was the result of admixture of detrital organic carbon, and that coupling was the norm in more organic-rich, shallow marine settings. These findings supported the primary nature of negative carbon isotope excursions, and lead to the prediction that shallower and organically more productive settings ought to exhibit closer isotopic coupling during isotope excursions. However, the existence of this postulated DOC reservoir has yet to be demonstrated using transects from shallow to deep marine settings.

The existence of an organic carbon reservoir would play a significant role in buffering oxygen levels (Rothman et al., 2003; Fike et al., 2006; Li et al, 2010, 2012, 2015; Swanson-Hysell et al., 2010). Organic carbon acts as an electron donor in redox reactions, while an organic carbon reservoir could potentially provide enough reductant capacity to sustain ocean redox stratification (Li et al., 2012, 2015; Fan et al., 2014). Oxygen levels, in general, are controlled by the balance between net oxidant flux (mostly from oxidative weathering and oxidation of volcanic outgassing) and net reductant flux (mostly from organic production). The presence of an organic carbon pool in the lower oceans would also generate a negative climate feedback,

whereby excess organic carbon production would be compensated by a greater net contribution from 'DOC' oxidation, releasing CO_2 and preventing further global cooling and glaciation (Swanson-Hysell et al., 2010). The magnitude and buffering capacity of the putative organic carbon reservoir would be tightly related to the stability and evolution of Earth's surface environment. However, its existence is hotly disputed, with some authors skeptical that enough oxidizing power could ever have been available to remineralise sufficient organic carbon to cause large carbon isotope perturbations (Bristow and Kennedy, 2008). As a result, the precise nature of the organic carbon reservoir is in dispute (Swanson-Hysell et al., 2010; Bjerrum and Canfield, 2011; Jiang et al., 2010; Johnston et al., 2012), while there is an overall lack of direct geological evidence (Jiang et al., 2012; Johnston et al., 2012). This study attempts to resolve this problem by comparing a shallow marine section with two other, more distal, but time-equivalent successions for the late Cryogenian warm interval (LCWI) in the Nanhua Basin.

The Nanhua Basin in South China is a suitable subject to study the evolution of the non-glacial Cryogenian ocean composition because of its well-characterized stratigraphic (glacigenic) framework, including upper and lower radiometric age constraints. The Datangpo Formation and correlative Xiangmeng Formation were both deposited between the late Cryogenian (Marinoan) glaciation and the early Cryogenian (Sturtian) glaciation in the Nanhua Basin, South China. Both the Datangpo and Xiangmeng formations comprise apparently complete, organic carbon-rich black shale and siltstone that make good subjects for studying the carbon

cycle and redox conditions between the Cryogenian glaciations. The organic carbon-rich nature of these units makes their $\delta^{13}C_{org}$ records more reliable, allowing us potentially to address questions such as: Did redox conditions govern the burial of organic carbon? Was there a carbon isotope gradient in the Cryogenian non-glacial ocean? What organic carbon sources contributed to the organic carbon isotope composition of deposited organic matter? The three drill cores examined in this study present the Datangpo Formation (=Xiangmeng Formation) in its entirety, developed in slope (Daotuo section), shallower basin (Minle section), and basin (Xiangtan section) settings. The depositional depth of Minle section is shallower than that of Xiangtan section (Fig. 1) (Jiang et al., 2011).

2 Geological setting and sample descriptions

The Neoproterozoic strata in South China were deposited in a rift to passive margin setting along the southeastern side of the Yangtze platform (Li et al., 1999; Jiang et al., 2003; Zhang et al., 2008), and are composed of three major parts (Jiang et al., 2003; Zhou et al., 2004; Zhang et al., 2008) (Fig.1): (1) pre-glacial siliciclastic rocks (Liantuo Formation and Banxi Group), being thin in the interior of the Yangtze Block and thick (>2 km) in the basin; (2) two Cryogenian-age, glacially-influenced diamictite intervals (Chang'an/Dongshanfeng/Tiesi'ao Formation and Nantuo Formation) that are separated by a manganese-bearing siltstone/shale unit (Datangpo/Xiangmeng Formation); and (3) post-glacial marine carbonates and

shales (Doushantuo Formation and Dengying/Liuchapo Formation) that are thick (>700m) on the shelf but thinner (<250m) in the basin. During the Cryogenian, the Yangtze platform can be divided into three sedimentary facies, representing different depositional environments from northwest to southeast: (1) platform facies; (2) slope facies; and (3) basin facies (Jiang et al., 2011).

The Datangpo/Xiangmeng Formation is sandwiched between two major glacially-influenced diamictites, the older Tiesi'ao Formation (Gucheng Formation in western Hunan Province) and the younger Nantuo Formation (Dobrzinski and Bahlburg, 2007; Zhang et al., 2008, 2013). The Datangpo Formation and the Xiangmeng Formation are time-equivalent Cryogenian non-glacial (warm interglacial) deposits.

Looking more widely, the Datangpo Formation and the Taishir Formation in western Mongolia were likely deposited around the same time (Fig. 2), while the Ombaatjie Formation of Namibia is probably equivalent to the upper portion of the Datangpo Formation (Hoffman, 2011). The Trezona Formation of Adelaide Rift Complex, South Australia is probably equivalent to the upper portion of the Datangpo Formation (McKirdy et al. 2001; Rose et al., 2012).

The Tiesi'ao Formation comprises diamictites, and is correlative with Sturtian glacigenic deposits globally (Zhang et al., 2003; Macdonald et al., 2010; Zhang et al., 2015). The Nantuo Formation comprises thick diamictites, siltstones, and sandstones, and is correlative with Marinoan glacigenic deposits globally (Condon et al., 2005; Zhang et al., 2005; Zhang et al., 2015). The Datangpo Formation and the Xiangmeng

Formation comprise the entire sedimentary record of the Nanhua Basin between the Sturtian and Marinoan glacial intervals.

The Daotuo, Minle and Xiangtan drill cores exhibit different facies and represent different depositional settings (Fig.1). The Daotuo section is located in Songtao County in northeastern Guizhou Province (N28°07′3.67″, E108°52′25.86″, Drill core ZK105). The Datangpo Formation is 285.5 m thick, representing a slope setting. The Daotuo section contains the thickest example of the Datangpo Formation in the Nanhua Basin. The Minle section is located in Huayuan County in western Hunan Province (Drill core 0905). At Minle section, the Datangpo Formation is 196.3 m thick, and represents a shallower basin setting. The Xiangtan section is located near Xiangtan City in Hunan Province (N27°58′31″, E112°50′22″, Drill core 0905), where the Xiangmeng Formation（=Datangpo Formation）is 89 m thick and represents a basin setting. The depositional depth of Xiangtan section is deeper than that of Minle section (Fig.1)(Jiang et al., 2011). Although of different thicknesses, the studied sections have a similar lithologic profile (Fig.2) with intervals of manganese carbonate, directly overlying Sturtian-age diamictites of the Gucheng or Tiesi'ao formations, followed by organic carbon-rich black shale (or gray-black shale), and gray siltstone (Li et al., 2012; Zhang et al., 2015). The Datangpo/Xiangmeng Formation exhibits an apparently conformable contact with both the underlying Tiesi'ao/Gucheng Formation as well as the overlying Nantuo Formation, and contain no intra-formational break in deposition (Fig.4) for the three studied drill cores.

Detailed lithologic information about the Daotuo section can be found in Zhang et al. (2015). The Datangpo Formation at Minle can be divided into 7 units (Fig.2). Unit 1 is a 1.3-m-thick layer composed of pyritic, Mn-carbonate. Unit 2 is a 3.8-m-thick layer composed of gray shale. Unit 3 is a 45.5-m-thick layer composed of black shale. Unit 4 is a 33.0-m-thick layer composed of black shale and gray shale. Unit 5 is a 69.0-m-thick layer composed of gray shale. Unit 6 is a 19.3-m-thick layer composed of black shale, gray shale. Unit 7 is a 24.4-m-thick layer composed of black-silty shale. The Xiangmeng Formation at Xiangtan can be divided into 4 units (Fig.2). Unit 1 is a 0.4-m-thick interval composed of Mn-carbonate. Unit 2 is a 82.0-m-thick interval composed of black shale. Unit 3 is a 1.1-m-thick interval composed of gray-black manganese-bearing limestone. Unit 4 is a 5.5-m-thick interval composed of a calcareous, pyritic, gray-black shale.

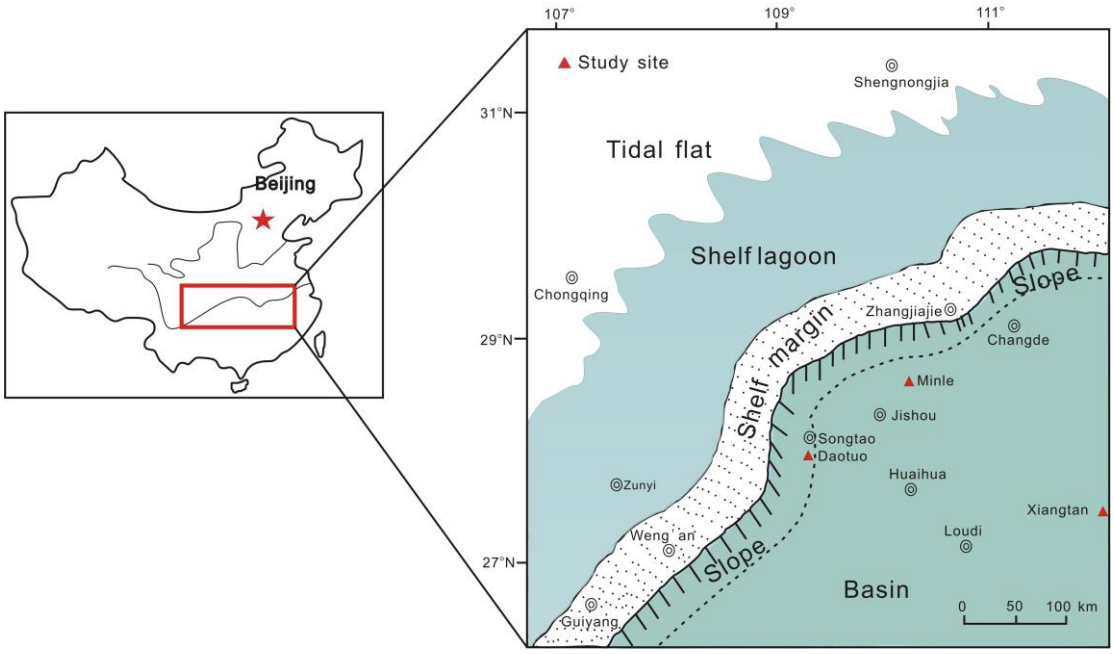

Fig. 1 A simplified paleogeographic map showing the studied area (modified Jiang et

al., 2011)

A

Era	Stage	Global glaciation	Eastern Guizhou, China	Northwestern Hunan, China	Tsagaan-olom Basin, Mongolia	Congo Craton, Namibia	Adelaide Rift Complex, Australia
Neoproterozoic	Cryogenian	Marinoan Glaciation	Nantuo Fm. 654.5±3.8 Ma (1)	Nantuo Fm.	Khongor Fm.	Ghaub Fm.	Elatina Fm.
			Datangpo Fm. 662.9±4.3 Ma (2)	Xiangmeng Fm.	Taishir Fm. 659.0±4.5Ma (3)	Ombaatjie Fm.	Trezona Fm.
						Gruis Fm.	
		Sturtian Glaciation	Tiesi'ao Fm.	Gucheng Fm.	Maikhan-Uul Fm.	Rasthof Fm.	Apilla Fm.
			Liangjiehe Fm.	Dieshuihe Fm.	Zavkhan Fm.	Chuos Fm.	

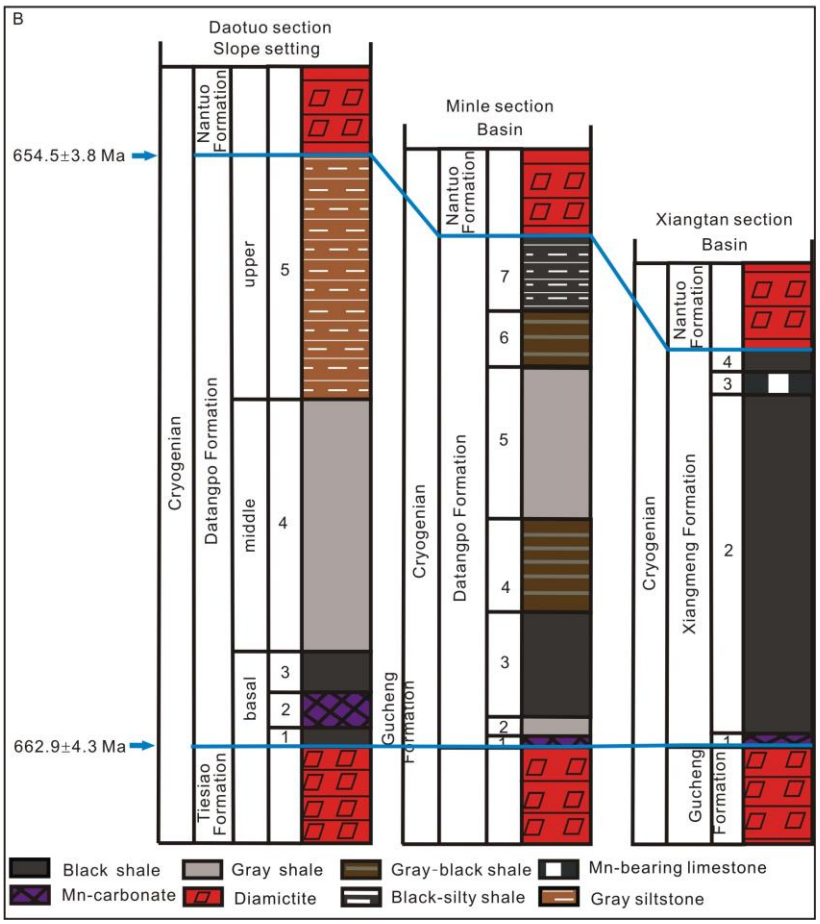

Fig. 2 A. Stratigraphic correlations of South China and Namibia, Mongolia during Cryogenian non-glacial stage. B. The stratigraphic column shows the stratigraphic succession of study sections. (1) SHRIMP zircon U-Pb age (Zhang et al., 2008). (2) Zircon U-Pb age (Zhou et al., 2004). (3) Re-Os isochron age (Rooney et al., 2015).

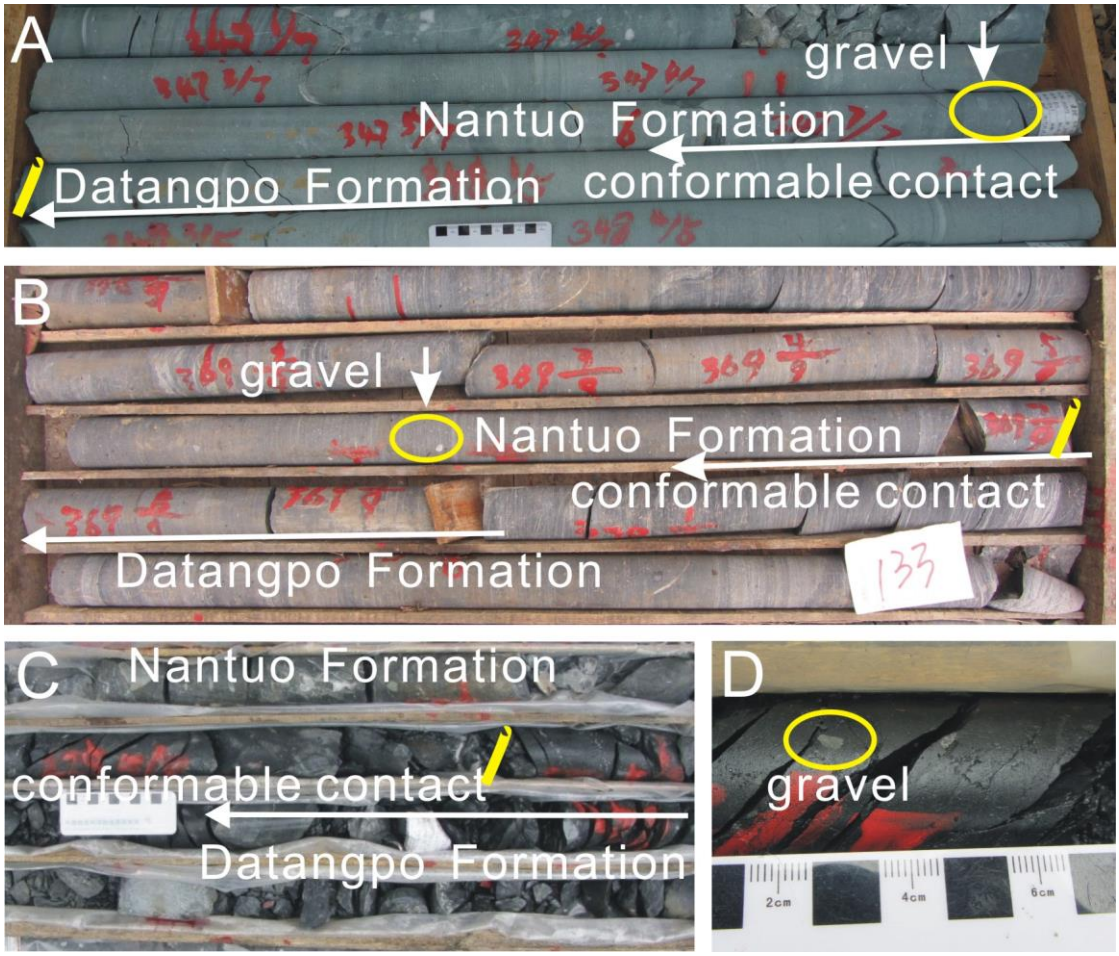

Fig.3 Drill core photographs. A. Gradual transition between Datangpo Formation and Nantuo Formation in the Daotuo section, Songtao County in northeastern Guizhou. B. Gradual transition between Datangpo Formation and Nantuo Formation with the presence in the Minle section, Huayuan County in western Hunan Province. C. Gradual transition between Datangpo Formation and Nantuo Formation in the Xiangtan section, Xiangtan City in Hunan Province. D. Gravels in top part of Xiangmeng Formation (black shale) in Xiangtan section.

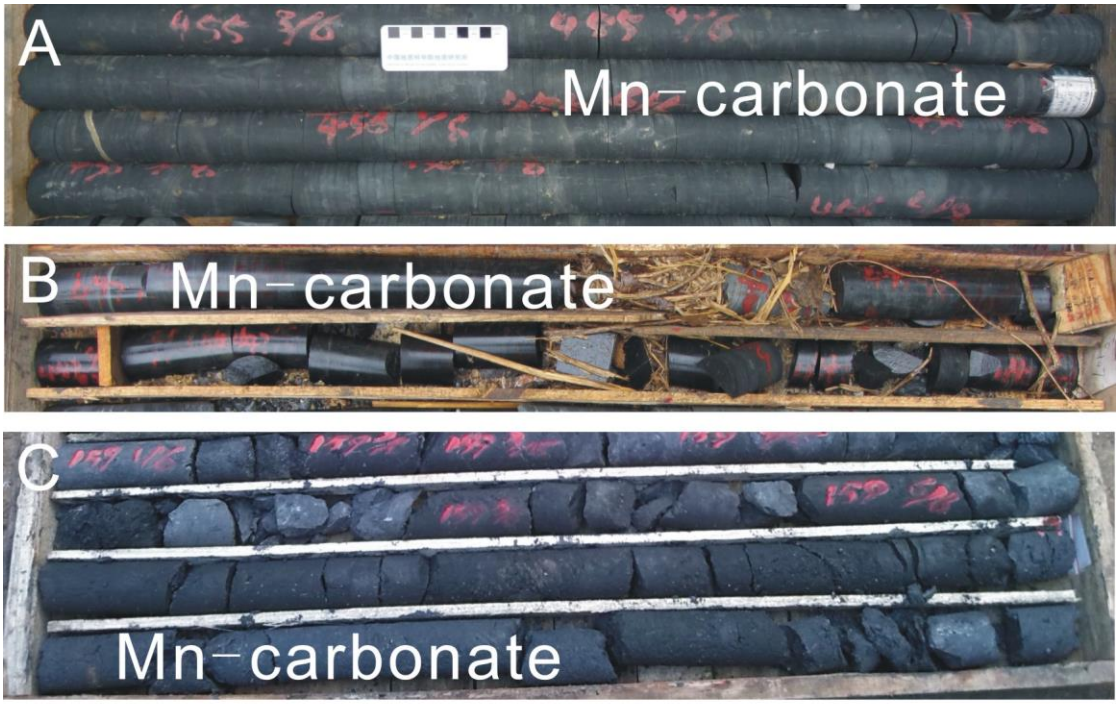

Fig.4 A. Strata containing Mn-carbonate ore in the Datangpo Formation for Daotuo section. B. Strata containing Mn-carbonate ore in the Datangpo Formation for Minle section. C. Strata containing Mn-carbonate in the Xiangmeng Formation for Xiangtan section.

3 Analytical methods

3.1 Major elements

Bulk-rock samples of various lithologies, including black shale, Mn-carbonate, grey shale, and grey siltstone, were prepared for geochemical analysis by washing in 18.2 Milli-Q H_2O and crushing to a powder. 153 samples were analyzed in a clean room at the National Research Center for Geoanalysis, Chinese Academy of Geological Sciences. Major elements were analyzed by ICP-AES (inductively coupled plasma–atomic emission spectrometry).

3.2 Organic carbon abundance and organic carbon isotopes

A total of 485 samples were analyzed for C isotope compositions in this study, of which, 259 samples were collected from Daotuo drill core at a spacing of 0.5-2.0m; 180 samples were collected from Minle drill core at a spacing of 0.1-2.0 m; and 46 samples were collected from Xiangtan section at a spacing of 0.5-4.0 m. For every sample, veins were avoided to avoid late-stage hydrothermal effects.

For each sample, ca.3g of fresh shale was ground to powder (200 mesh) in an automated agate mill. Samples were decalcified with concentrated HCl (6M) for 1h at 70°C, buffered back to about neutral pH (>pH5) with deionized water, then centrifuged and the supernatant removed. The siliciclastic content was removed with HF (6M) for 1h (70 °C). Samples were buffered back to about neutral pH (>pH5) with deionized water again, centrifuged, and the supernatant removed and evaporated to dryness at 50°C. Homogenized residues were analyzed on a Vario EL cube elemental analyzer for TOC contents, and on a ThermoFinnigan Delta XL Plus in continuous mode for C isotope compositions. External and internal uncertainties were monitored using urea standards, and were better than 0.1% and 0.2‰ for TOC and $\delta^{13}C_{org,}$ respectively. To monitor the reproducibility, duplicates were analyzed for every sample. All isotope values are reported as δ values with reference to the Vienna Pee Dee Belemnite standard (VPDB).

Sample preparation was performed in the MLR Key Laboratory of Isotope Geology, Institute of Geology, Chinese Academy of Geological Sciences, and sample analyses carried out in the State Key Laboratory of Organic Geochemistry,

Guangzhou Institute of Geochemistry, Chinese Academy of Sciences.

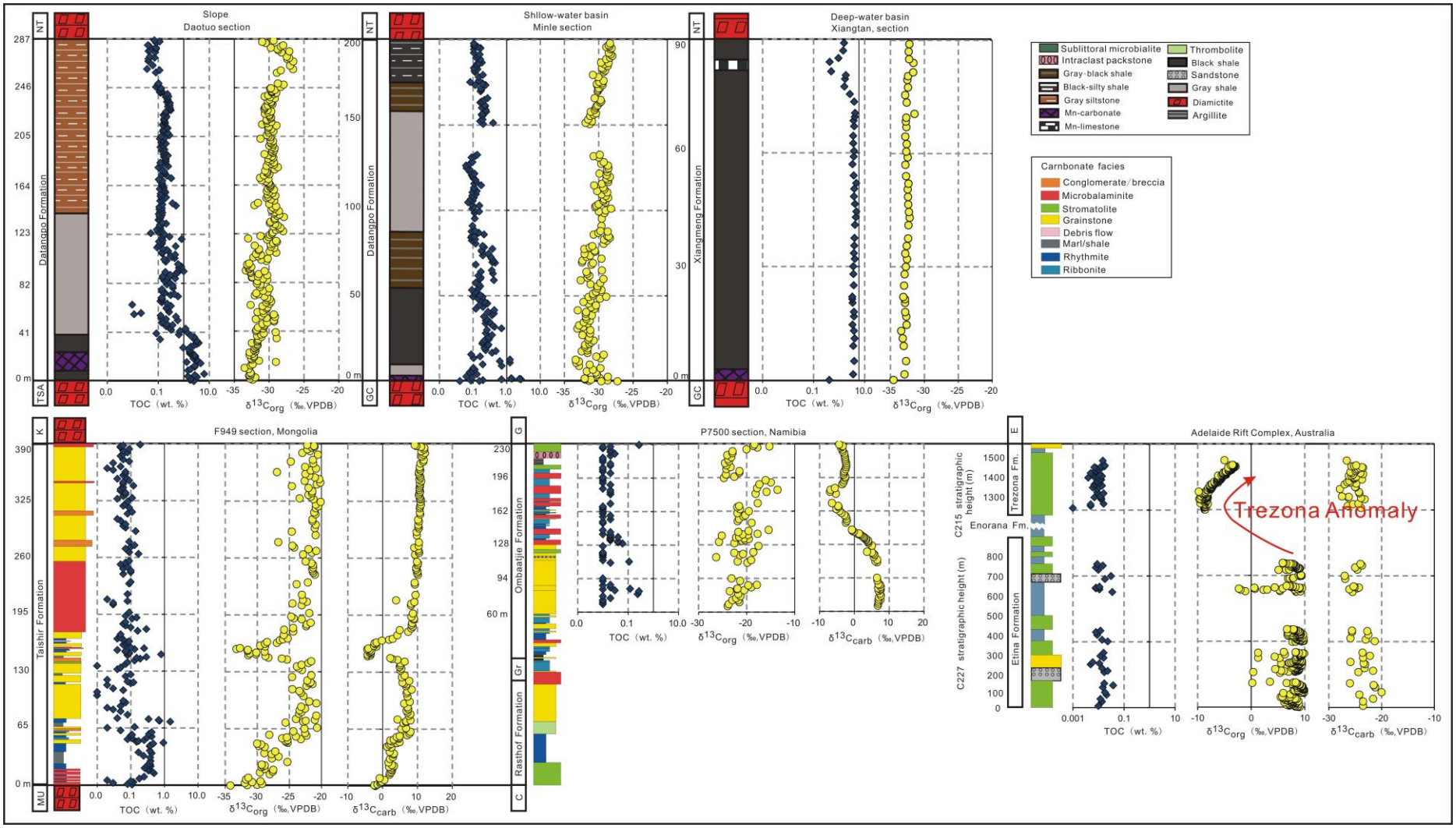
Slope
Daotuo section
Shllow-water basin
Minle section
Deep-water basin
Xiangtan, section
Datangpo Formation
Xiangmeng Formation
NT
TSA
GC
TOC（wt. %）
δ13Corg（‰,VPDB）
Sublittoral microbialite
Intraclast packstone
Gray-black shale
Black-silty shale
Gray siltstone
Mn-carbonate
Mn-limestone
Thrombolite
Black shale
Sandstone
Gray shale
Diamictite
Argillite
Carnbonate facies
Conglomerate/breccia
Microbalaminite
Stromatolite
Grainstone
Debris flow
Marl/shale
Rhythmite
Ribbonite
F949 section, Mongolia
Taishir Formation
Ombaatjie Formation
Rasthof Formation
K
MU
G
Gr
C
δ13Ccarb（‰,VPDB）
P7500 section, Namibia
Adelaide Rift Complex, Australia
E
Trezona Fm.
Enorana Fm.
Etina Formation
C215 stratigraphic height (m)
C227 stratigraphic height (m)
Trezona Anomaly

Fig. 5 Spatial and temporal distribution of organic carbon isotopes and TOC abundance. Data for F949 section for the Taishir Formation and P7500 section are from Johnston et al. (2012). F949 section is located at Uliastay Gol, Mongolia (46°49′30″N, 95°49′20″E). P7500 section is located at Namibia (19°09′26″S, 13°51′09″E). Data for C215 and C227 section are from Swanson-Hysell et al. (2010). C215 and C227 section are located at Adelaide Rift Complex, Australia (31°23′44″S, 138°51′14″E). C indicates the Chuos Formation. E indicates the Marinoan-equivalent Etina Formation. G indicates the Ghaub Formation, and Gr indicates the Gruis Formation. GC indicates the Sturtian-equivalent Gucheng Formation. MU indicates the Sturtian-equivalent Maikhan-Uul Formation, and K indicates the Marinoan-equivalent Khongor Formation. TSA indicates the Sturtian-equivalent Tiesi'ao Formation, and NT indicates the Marinoan-equivalent Nantuo Formation.

4 Results

The results of major element content, TOC abundance and $\delta^{13}C_{org}$ results for the study sections are listed in Table 1 of the supplementary material.

Daotuo section (slope setting)

The TOC abundance ranges from 0.01 wt.% (at 41 m and 51 m) to 6.35 wt.% (at 3.8 m), averaging 0.52 ±0.88 wt.%. $\delta^{13}C_{org}$ ranges from -33.5‰ (at 4.8 m) to -26.5‰ (at

261.5 m), averaging -30.3 ±1.4‰. TOC abundance decreases through the non-glacial interval, from 2.48 wt.% to 0.10 wt.% (Fig.5), while $\delta^{13}C_{org}$ values clearly show two successive increasing trends, and an overall increase from -32.3‰ at the base to -29.3‰ at the top. There are also two $\delta^{13}C_{org}$ excursions (ca. 5‰) at the bottom of the Daotuo section. At Daotuo, changes in TOC abundance and lithology are synchronous, but changes in organic carbon isotopes and lithology do not coincide (Fig.5).

Minle section (shallower basin setting)

The TOC abundance ranges from 0.04 wt.% (at 0 m) to 2.67 wt. % (at 1.0 m), averaging 0.24 ±0.32 wt.%. $\delta^{13}C_{org}$ ranges from -33.4‰ (at 14.4 m) to -27.3‰ (at 0 m), averaging -30.3 ±1.3‰. TOC abundance is higher after Sturtian Glaciation than before Marinoan Glaciation, from 2.67 wt. %to 0.11 wt. %. And $\delta^{13}C_{org}$ values show an obvious increasing trend during the non-glacial interval, from -32.0‰ to -28.3‰ (Fig.5). There was a $\delta^{13}C_{org}$ excursion (ca. 4‰) at the bottom of Minle section. But the change to and away from the nadir is more muted compared with that of Daotuo section (Fig.5). For Minle section, TOC abundance and organic carbon isotope values are variable at the bottom and stable for the middle and upper part, while lithology is variable for the whole section (Fig.5).

Xiangtan section (basin setting)

The TOC abundance is relatively high, ranging from 0.42 wt.% (at 0 m) to 4.80 wt.%

(at 44.5 m), averaging 3.32 ±1.16 wt.%. $\delta^{13}C_{org}$ ranges from -34.5‰ (at 0 m) to -31.4‰ (at 70.5 m), averaging -32.6 ±0.5‰. TOC abundance decreases sharply at 81.5 m, from 2.67 wt. % to 0.50 wt. % (Fig.5), but $\delta^{13}C_{org}$ remains stable through the whole profile, being -32.9‰ at the base and -32.3‰ at the top. Lithology remains unchanged despite the major decrease in TOC near the top of the formation (Fig.5).

5 Discussion

5.1 Geochronological constraints on the Datangpo/ Xiangmeng Formation

It is generally considered that the Nantuo deposits are equivalent to the global end-Cryogenian or 'Marinoan' glaciation (Condon et al., 2005; Zhu et al., 2007; Zhang et al., 2008). Thus, the Datangpo/Xiangmeng Formation covers the whole interval of the late-Cyogenian warm interval between the 'Snowball Earth' events. Most radiometric age data for Cryogenian strata were obtained from the Yangtze Block. A U-Pb age of 662.9 ± 4.3 Ma has been obtained from a layer of volcanic ash near the base of the Datangpo Formation (Zhou et al., 2004), which is regarded as an anchor for the termination of 'Sturtian' glaciation (Rooney et al., 2014, 2015). A U-Pb zircon study of tuffaceous beds from the top Datangpo Formation yield an age of 654.5 ± 3.8 Ma (Zhang et al., 2008). Thus, the Datangpo/Xiangmeng Formation covers a time interval of ca. 10 million years.

5.2 Chronostratigraphic correlation between the three sections

The relative completeness of the studied Datangpo and Xiangmeng formations is vital to interpretations of these isotope data. It is considered that considerable erosion must have occurred across a large area due to the postulated sea-level fall of up to 800 meters caused by the 'Marinoan' glaciation (Hoffman, 2005; Liu and Peltier 2013). Indeed, there are differences in thickness and lithology for the three studied sections that might be attributed to erosional truncation. This issue is dealt with specifically below by examining the nature of the contacts between underlying and overlying strata.

5.2.1 Contact relationship with underlying strata

Mn-carbonate ore is a unique feature that is characteristic of the Datangpo Formation (Xiangmeng Formation) across the Yangtze platform (Fig.4). It has been well documented that the Mn-carbonate ore-bearing strata occur at the bottom of the Datangpo and Xiangmeng formations in both outcrop sections and drill cores (Fan et al., 1992; Zhou et al.， 2004；Zhang et al., 2015; Wu et al., 2016). As shown in Figs. 2 and 4, Mn-carbonate beds have been observed to mark the base of the non-glacial succession at each of the three localities studied here (Fig.2). This suggests that the non-glacial sedimentation of the Datangpo/Xiangmeng Formation occurred almost synchronously in the three localities, and that there is no significant hiatus between the non-glacial and underlying glacial sedimentation.

5.2.2 Contact relationship with overlying strata

The base of the Nantuo Formation is marked by the onset of conglomerate (diamictite) deposition (Zhang et al., 2008). Although the transitions between the Datangpo (Xiangmeng) Formation and the Nantuo Formation are generally sharp, no discontinuities are observed at any of the three sections (drill cores in the three areas) (Fig.3). Instead, gradational transitions between the two formations are evident in terms of their colour, organic content and general lithology (Fig.3). More importantly, angular gravels have been observed at the top of the Xiangmeng Formation in some drill cores (Fig.3C, D). The large sizes of the gravels are in great contrast to those of the host black shale (Fig. 3A, B, C, D). Thus, these gravel lonestones are considered to be possible dropstones. The occurrence of outsized dropstones in otherwise, very fine-grained black shale argues for continuity of sedimentation between the Datangpo/Xiangmeng Formation and the overlying Nantuo diamictite. Therefore, the Xiangtan black shale is argued to cover the entire non-glacial interval in South China.

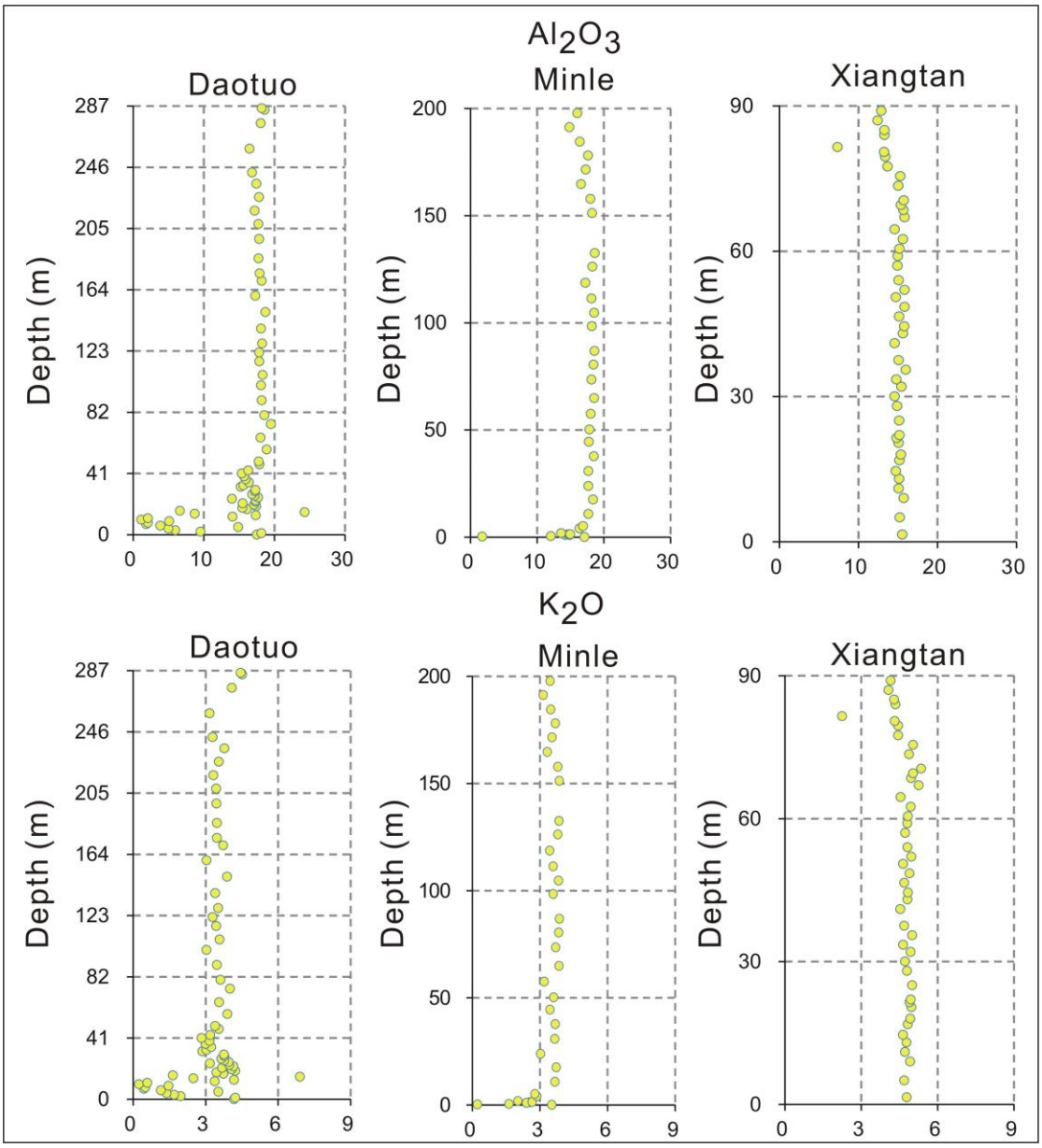

Fig.6 Comparisons between Al_2O_3 and K_2O contents in Daotuo, Minle and Xiangtan dill core sections

5.3 Constraints on the depositional settings

Although samples from different depositional settings were purposely selected, using previous studies as a guide, it is important to examine whether features exhibited by the studied samples are consistent with their supposed settings.

5.3.1 Grain sizes

Sediment grain size can reflect hydrodynamic conditions. Coarse grain size is taken to indicate a high energy (high velocity) environment, while fine grain size suggests low energy (low velocity) conditions. Therefore, grain size distribution can also reflect sedimentary depth (Ghoshal et al., 2010; Bouchez et al., 2011). The Datangpo Formation at Daotuo is mainly composed of black shale and siltstone, with the portion of siltstone being much larger than that of shale. This is consistent with the the Datangpo Formation at Daotuo being situated nearer the land. The Datangpo Formation at Minle is mainly composed of black shale, gray shale and a little siltstone, indicating that the depositional site for the Datangpo Formation at Minle was further away from its terrestrial source than for Daotuo, thus likely deeper. The Xiangmeng Formation in Xiangtan is mainly composed of fine black shale, which indicates a quiet depositional environment. Thus, compared with the Datangpo Formation at Daotuo and the Datangpo Formation at Minle, the Xiangmeng Formation at Xiangtan was likely deposited in the deepest part of the basin.

5.3.2 Clay minerals

Clay minerals can be transported a long distance. Clay minerals generally contain a mixture of some or all of kaolinite, illite, smectite and chlorite, depending on the depositional setting. Kaolinite settles more quickly, followed by illite, due to their different hydrodynamic properties (Thiry et al., 2000; Kalinenko, et al., 2001). Therefore, kaolinite is found in greater abundance near the shore, while illite

concentrations increase in a relative sense away from shore. The obvious difference between kaolinite and illite is the abundance of potassium (K). Illite is rich in K, and kaolinite lacks K. Compared with samples from Daotuo and Minle, Xiangtan samples are rich in K_2O, which indicates that Xiangtan is rich in illite (Fig.6), thus providing further support that the Xiangtan strata were deposited in a deeper marine environment than those at Daotuo and Minle.

5.3.3 Sedimentation rates

The greater thickness of the Datangpo Formation at Daotuo is consistent with the greater abundance of terrestrially-derived material and high sedimentation rates expected of a nearshore environment. Conversely, being most distal from the shore, it might be expected that the Xiangmeng Formation at Xiangtan would be relatively condensed due to a relative lack of terrestrially-derived material and lower sedimentation rate. The thickness of the Datangpo Formation at Minle is between these two extremes.

Based on grain size, clay mineral distributions and sedimentation rates, we propose that the order of depositional depth for the study sections is: Daotuo < Minle < Xiangtan.

5.4 Temporal and spatial variability of organic carbon isotope composition

Organic carbon isotopic values obtained in this study vary according to depositional

setting in the Nanhua Basin, South China (Fig.1). Firstly, from the nearshore, slope setting to the more distal deep-water basin, average TOC abundances show an obvious increase, from 0.52 wt.% to 3.32 wt.%; and average $\delta^{13}C_{org}$ values show a significant decrease (Fig.5), from -30.3‰ to -32.6‰. Secondly, $\delta^{13}C_{org}$ values exhibit an increasing trend with time after the 'Sturtian' glaciation towards the 'Marinoan' glaciation, especially at Daotuo and Minle. Thirdly, significant negative $\delta^{13}C_{org}$ excursions are evident in the slope and shallow-water basin environments: ca. 5‰ at Daotuo and ca. 4‰ at Minle. By contrast, the $\delta^{13}C_{org}$ values at Xiangtan are unchanging. The spatial distribution of $\delta^{13}C_{org}$ values indicates a depth gradient in the isotopic composition of the organic carbon fraction of deposited sediments in the Cryogenian non-glacial warm interval ocean.

5.5 Main possible interpretations for the distributional features of TOC abundance and $\delta^{13}C_{org}$

The spatial distribution of $\delta^{13}C_{org}$ and TOC abundance from our study shows that $\delta^{13}C_{org}$ values decrease with depth, while TOC abundance increases with depth (Fig.5). $\delta^{13}C_{org}$ values increase with time at Daotuo and Minle, but remain unchanging at Xiangtan (Fig.5). The $\delta^{13}C_{org}$ data can reflect carbon sources and redox conditions. The most likely reasons causing the apparent organic carbon isotope gradient include: (1) admixture of detrital organic carbon with primary production (Jiang et al., 2012; Johnston et al., 2012); (2) biological pump (Shen et

393 a1., 2005; Gidding and Wallace, 2009); (3) diagenetic alteration (Gidding and
394 Wallace, 2009; Jiang et al., 2012; Wang et al., 2016); (4) admixture of organic
395 material from an 'dissolved' or 'particulate' organic carbon reservoir (Rothman et al.,
396 2003).

397 **5.5.1 The effect of detrital organic carbon is insignificant**

398 Detrital organic carbon, primary production and secondarily recycled primary
399 production (particularly bacteria biomass) are major sources of TOC in marine
400 sediment (Jiang et al., 2012). Terrestrial organic carbon is mainly of low abundance
401 (Burdige, 2007; Campbell and Squire, 2010) and so the contribution of detrital
402 carbon in the black shales of the Xiangmeng Formation and lower parts of the
403 Datangpo Formation is unlikely to be significant. Furthermore, the contribution of
404 terrestrial organic carbon would be expected to decrease with increasing distance
405 from the shore. However, TOC abundance at the deeper Xiangtan section is much
406 higher than that at either Daotuo or Minle (Fig.5). Therefore, it can be concluded that
407 the effect of detrital organic carbon is insignificant in our samples.

408 **5.5.2 Primary productivity and biological pumping cannot explain the overall**
409 **organic carbon abundance and $\delta^{13}C_{org}$ distribution.**

410 Primary production is controlled by the abundance of nutrients, such as nitrogen and
411 phosphorus. Rivers bring abundant nutrients to the ocean (Bernard et al., 2011), and
412 detrital abundance decreases in general with increasing distance from the shore.

Therefore, the contribution that primary producers make to TOC achieves its high point in the slope environment due to the abundant nutrients from terrestrial sources and upwelling waters (Falkowski et al., 1998). This is inconsistent with the observed TOC distribution in our study (Fig.5). The contribution of chemoautotrophic biomass is the same with that of primary production.

Biological pumping results from preferential uptake of ^{12}C by primary producers and remineralization of the ^{12}C-rich organic matter at depth, which leads to shallow DIC enriched in ^{13}C and deep DIC enriched in ^{12}C (Shen et al., 2005; Gidding and Wallace, 2009). Biological pumping can cause primary producers at different depths to incorporate dissolved inorganic carbon of different $\delta^{13}C$, this does not necessarily lead to a $\delta^{13}C_{org}$ gradient. In any case, any effect from biological pumping cannot explain the temporal trends in $\delta^{13}C_{org}$.

5.5.3 Early diagenetic alteration is not a sigificant factor

Bacterial sulphate reduction and methanogenesis are the main microbially-driven reactions during early diagenesis (Gidding and Wallace, 2009). The intense activity of chemoautotrophic and methanotrophic bacteria can cause $\delta^{13}C_{org}$ values in organic matter to become more negative (Summons et al., 1998; Hollander and Smith, 2001; Jiang et al., 2010, 2012). The prerequisites for the activity of chemoautotrophic and methanotrophic bacteria are anoxic conditions and abundant organic matter. Biomass of chemoautotrophic and methanotrophic bacteria could make significant contributions to both the $\delta^{13}C_{org}$ negative shift of the basal part at Daotuo and Minle,

as well as the decreasing trend in $\delta^{13}C_{org}$ with depth. However, the activity of chemoautotrophic and methanotrophic bacteria alone cannot explain the overall increasing trend in $\delta^{13}C_{org}$ and/or lack of marked fluctuations in absolute values. Consequently, the effects of early diagenesis are unlikely to be significant for the purposes of our study and can be neglected.

5.6 A deep marine organic carbon reservoir in a gradually oxygenating ocean

As discussed above, any dominant effect from detrital organic carbon and primary producers on the organic carbon cycle in the studied area can be ruled out. The biological pumping and activity of chemoautotrophic and methanotrophic bacteria rely on abundant organic carbon, and their effects cannot explain the overall $\delta^{13}C_{org}$ trends. In contrast, the existence of a deep marine organic carbon reservoir in a redox-stratified ocean can plausibly explain the temporal and spatial distribution of $\delta^{13}C_{org}$ and TOC abundance. In our study, the deepest depositional environment is associated with greater TOC and more negative $\delta^{13}C_{org}$ values. This organic carbon source is akin to the dissolved organic carbon (DOC) reservoir proposed by Rothman et al. (2003), although the distinction between recalcitrant dissolved and particulate organic matter is not central to the arguments below (Jiao et al., 2010; Liu and Peltier, 2011; Hansell, 2013). It is envisaged that DOC could adsorb on, or aggregate with settling clays in areas of relatively low primary production, thus dominating the organic carbon isotope signature in those settings.

It has been documented that the Cryogenian Nanhua ocean became gradually

oxygenated during the Datangpo interval (Li et al., 2012; Zhang et al., 2015). The $\delta^{13}C_{org}$ values at Daotuo and Minle increase with time, which is consistent with enhanced organic carbon burial and oxygen production. The almost unchanging $\delta^{13}C_{org}$ values for Xiangtan are anomalous and could be caused by a greater relative contribution from 'old' carbon out of the deep ocean organic carbon reservoir, and is consistent with redox-stratification during most of the mid-Cryogenian non-glacial interval in the Nanhua Basin (Shields et al., 1997, 2002; Li et al., 2012). The organic carbon is predisposed to build the organic carbon reservoir. As the net growth of the organic reservoir surpassed its peak (high $\delta^{13}C$), and began to oxidise, negative $\delta^{13}C$ anomalies in the shallow marine DIC reservoir and in organic matter produced at shallow depths in the ocean would be predicted to reflect this oxidation.

The observation that the $\delta^{13}C_{org}$ values at Daotuo, Minle and Xiangtan decrease with depth can be explained, therefore, by the increasing effect of the deep marine organic carbon reservoir at greater depths. Small negative shifts in $\delta^{13}C_{org}$ in the basal parts of Daotuo and Xiangtan could have been caused by influx from organic carbon reservoir through ocean upwelling (Fan et al., 2014). Based on the above analysis, it is suggested that there was a large organic carbon reservoir in the Nanhua Basin during mid-Cryogenian (non-glacial), warm interval, and the ocean is gradually oxygenated and redox stratified.

5.7 The effect of a long-lived marine organic carbon reservoir on the carbon cycle during the Cryogenian non-glacial interval

The organic carbon reservoir would have helped to buffer oxygen levels on the Earth's surface, and would also have affected the concentration of CO_2 in the atmosphere. Hence, research on the deep marine organic carbon reservoir is critical to exploring the evolutionary history of life and its planetary environment. Decoupling between $\delta^{13}C_{carb}$ and $\delta^{13}C_{org}$ was used to confirm the existence of the DOC reservoir during the Ediacaran Period (Fike et al., 2006; McFadden et al., 2008). Swanson-Hysell et al. (2010) found that there was complete decoupling between $\delta^{13}C_{carb}$ and $\delta^{13}C_{org}$ during the Cryogenian non-glacial interval, which was argued to be in accord with the existence of a huge DOC reservoir. In contrast, Johnston et al. (2012) proposed a quantitative mixing model to explain coupled and decoupled $\delta^{13}C_{carb}$ and $\delta^{13}C_{org}$ data from Mongolia and Canada, and from Namibia, respectively, and did not support existence of a DOC reservoir during the Cryogenian non-glacial interval. Does the model of a gradually oxygenating, redox-stratified ocean with a large, deep-ocean, organic carbon reservoir proposed in this study accord with the $\delta^{13}C_{org}$ data from other areas during Cryogenian non-glacial interval?

To date, three complete $\delta^{13}C_{carb}$ records (the Taishir Formation in Tsagaan-Olom basin, southwestern Mongolia, and Nepouie and Upalinna Subgroups in south Australia), one complete $\delta^{13}C_{org}$ record (the Taishir Formation in Tsagaan-Olom basin, southwestern Mongolia), and three composite profiles of $\delta^{13}C_{carb}$ data (the

496 Taishir Formation in Dzabkhan Basin, Mongolia; Abenab Subgroup in Namibia)
497 have been presented for the mid-Cryogenian non-glacial, warm interval (Hoffman
498 and Schrag, 2002; Halverson et al., 2002, 2005; Giddings and Wallace, 2009;
499 Johnston et al., 2012; Bold et al., 2015, 2016).

500 There is a $\delta^{13}C_{carb}$ negative excursion in the basal part of the F949 section in the
501 Taishir Formation (Taishir Formation in Dzabkhan Basin, Mongolia), and a negative
502 excursion (ca. 10‰) occurs in the corresponding $\delta^{13}C_{org}$ record (Fig.5). There are
503 also $\delta^{13}C_{carb}$ and $\delta^{13}C_{org}$ negative excursions in the basal part of the P7500 section in
504 the Ombaatjie Formation (Congo Craton, Namibia) (Fig.5). The negative $\delta^{13}C_{carb}$
505 excursions are thought to have resulted from remineralization of primary production
506 and exogenous (detrital organic carbon) (Johnston et al., 2012), who argued against
507 any dominant effect from the marine organic carbon reservoir. However, studied
508 sections in Johnston et al. (2012) represent a much shallower marine environment
509 than sections in this study. The organic carbon reservoir existed in the deep sea, and
510 so its effect on the ocean carbon cycle would have decreased with increasing
511 distance from the shore. Moreover, the redox conditions would be different within a
512 redox stratified ocean. Shallow marine environments would be more oxic than
513 contemporaneous deep marine settings. The major organic carbon source might be
514 primary producers in the F949 section, but when upwelling brings dissolved organic
515 carbon from the deep organic carbon reservoir, the ‘old’ organic carbon can play a
516 more important role. The negative excursions of $\delta^{13}C_{carb}$ and $\delta^{13}C_{org}$ are likely to
517 have been caused by oxidation of organic carbon from the organic carbon reservoir

518 (Gidding and Wallace, 2009; Fan et al., 2014). The negative $\delta^{13}C_{carb}$ excursion in the
519 P7500 section may, by contrast, have been affected by 'detrital' or 'older' organic
520 carbon, and therefore there is no corresponding $\delta^{13}C_{org}$ negative excursion.

521 Is the Trezona anomaly present in the Nanhua Basin? If there was a
522 contemporaneous carbonate sedimentary record, then we should be able to recognize
523 the Trezona anomaly in the shallower parts of the basin. However, there are no
524 carbonate rocks of that age in South China, while no corresponding negative $\delta^{13}C_{org}$
525 excursion can be found in our data. For Daotuo section, the upper part was more oxic,
526 and $\delta^{13}C_{carb}$ negative excursion could appear due to oxidation of 'old' organic carbon
527 but no $\delta^{13}C_{org}$ negative excursion. Compared with Daotuo section, the upper part of
528 Minle section was less oxic, both $\delta^{13}C_{carb}$ and $\delta^{13}C_{org}$ negative excursion could occur
529 due to the effect of 'old' organic carbon (Fig.5). Xiangtan section was reducing, so
530 the Trezona anomaly could not occur.

531 It can be concluded that the dominant organic carbon sources and redox
532 conditions vary significantly during the Neoproterozoic, and this should be
533 considered when discussing the Neoproterozoic carbon cycle. With reference to our
534 proposed chemo-oceanographic structure: the existence of a large organic carbon
535 reservoir in the deeper parts of a periodically oxygenating and redox-stratified ocean
536 seems to us a reasonable way to view the non-glacial carbon cycle during the
537 Cryogenian Period.

538

6 Conclusions

Three complete $\delta^{13}C_{org}$ records for the Datangpo Formation (= Xiangmeng Formation) representing different depositional settings are presented in this study. The spatial and temporal variability of organic carbon isotopes is in accordance with the existence of a large organic carbon reservoir, which existed in the deep sea. The mid-Cryogenian non-glacial interval can be viewed as a time when the oceans beneath the pycnocline became rich in organic carbon, which underwent periodic net oxidation under redox-stratified conditions. The existence of an organic carbon reservoir can explain the evolution of organic carbon isotopes in the Dzabkhan Basin, Mongolia and Congo Craton, Namibia as well as Flinders Ranges, South Australia. This study seeks to demonstrate the significance of organic carbon isotopes in building a general framework towards a better understanding of the ocean structure during the Neoproterozoic. Studies of complete, high resolution $\delta^{13}C_{org}$ records in different depositional settings (from slope setting to deep-marine) help us to build a more detailed picture of the carbon cycle and redox conditions in the Nanhua Basin during mid-Cryogenian non-glacial, warm interval.

Acknowledgements

This study was financially supported by the Natural Science Foundation of China (Grant No. 41430104), the MLR Public Benefit Research Foundation (Grant No. 201411044), and the State Key Laboratory of Organic geochemistry Fund (Grant

560 No.OGL-201416). We are grateful to Engineer Jiazhuo He and Engineer Huashan
561 Chen for their assistance during the determination of TOC abundance and organic
562 carbon isotopic composition.
563

564 **References**

565 Bernard, C.Y., Dürr, H.H., Heinze, C., et al., 2011. Contribution of riverine nutrients
566 to the biogeochemistry of the global ocean-a model study. Biogeoscience 8:
567 551-564.
568 Bjerrum, C.J., Canfield, D.E., 2011. Towards a quantitative understanding of the late
569 Neoproterozoic carbon cycle. Proceedings of the National Academy of Sciences of
570 the United States of America 108(140), 5542-5547.
571 Bold, U., Smith, E.F., Rooney, A.D., et al., 2016. Neoproterozoic stratigraphy of the
572 Zavkhan Terrane of Mongolia: the backbone for Cryogenian and Early Ediacaran
573 chemostratigraphic records. American Journal of Science 316, 1-63.
574 Bold, U., Macdonald, F.A., Smith, E.F., et al., 2015. Elevating the Neoproterozoic
575 Tsagaan-Olom from Formation to Group. Mongolian Geoscientist 39, 89-94.
576 Bristow, T.F., Kennedy, M.J., 2008. Carbon isotope excursions and the oxidant
577 budget of the Ediacaran atmosphere and ocean. Geology 36, 863-866.
578 Burdige, D.J., 2007. Preservation of organic matter in marine sediments: controls,
579 mechanisms, and an imbalance in sediment organic carbon budgets?. Chemical
580 Review 107, 467-485.

581 Bouchez, J., Gaillardet, J., France-Lanord, C., et al., 2011. Grain size control of river
582 suspended sediment geochemistry: Clues from Amazon River depth profiles.
583 Geochemisry Geophysics Geosystems 12(3), Q03008.
584 Campbell, I.H., Squire, R.J., 2010. The mountains that triggered the Late
585 Neoproterozoic increase in oxygen: The Second Great Oxidation Event.
586 Geochimica et Cosmochimica Acta 74 (15), 4187-4206.
587 Canfield, D.E., Poulton, S.W., Narbonne, G.M., 2007. Late-Neoproterozoic
588 Deep-Ocean Oxygenation and the Rise of Animal Life. Science 315, 92-95.
589 Chen, X., Ling, H.-F., Vance, D., et al., 2015. Rise to modern levels of ocean
590 oxygenation coincided with the Cambrian radiation of animals. Nature
591 Communications 6, 7142.
592 Condon, D., Zhu, M., Bowring, S., 2005. U-Pb ages from the Neoproterozoic
593 Doushantuo Formation, China. Science 308, 95-98.
594 Dobrzinski, N., Bahlburg, H., 2007. Sedimentology and environmental significance
595 of the Cryogenian successions of the Yangtze Platform, South China block.
596 Palaeogeography, Palaeoclimatology, Palaeoecology 254, 100-122.
597 Falkowski, P.G., Barber, R.T., Smetacek, V., 1998. Biogeochemical controls and
598 feedbacks on Ocean Primary Production. Science 281, 200-206.
599 Fan, D., Liu, T., Ye, J., et al., 1992. The process of formation of manganese
600 carbonate deposits hosted in black shale series. Economic Geology 87, 1419-1429.
601 Fan, H., Zhu, X., Wen, H., et al., 2014. Oxygenation of Ediacaran Ocean recorded by
602 iron isotopes. Geochimica et Cosmochimica Acta 140, 80-94.

603 Fike, D.A., Grotzinger, J.P., Pratt, L.M., et al., 2006. Oxidation of the Ediacaran
604 Ocean. Nature 444(7), 744-747.
605 Frei, R., Gaucher, C., Poulton, S.W., et al., 2009. Fluctuations in Precambrian
606 atmospheric oxygenation recorded by chromium isotopes. Nature 461, 250-253.
607 Ghoshal, K., Mazumder, B.S., Purkait, B., et al., 2010. Grain-size distributions of
608 bed load: Inferences from flume experiments using heterogenerous sediment bed.
609 Sedimentary Geology 223, 1-14.
610 Giddings, G.A., Wallace, M.W., 2009. Facies-dependent $\delta^{13}C$ variation from a
611 Cryogenian platform margin, South Australia: evidence for stratified
612 Neoproterozoic oceans? Palaeogeography Palaeoclimatology Palaeoecology 271,
613 196-214.
614 Grotzinger, J.P., Fike, D.A., Fischer, W.W., 2011. Enigmatic origin of the
615 largest-known carbon isotope excursion in Earth's history. Nature Geoscience 4,
616 285-292.
617 Halverson, G.P., Hoffman, P.F., Schrag, D.P., 2002. A major perturbation of the
618 carbon cycle before the Ghaub glaciation (Neoproterozoic) in Namibia: Prelude to
619 snowball Earth?. Geochemistry, Geophysics, Geosystems 3(6), 1035.
620 Halverson, G.P., Hoffman, P.F., Schrag, D.P., et al., 2005. Toward a Neoproterozoic
621 composite carbon-isotope record. GSA Bulletin 117(9/10), 1181-1207.
622 Halverson, G.P., Shields- Zhou, G., 2011. Chemostratigraphy and the Neoproterozoic
623 glaciations, in: The Geological Record of Neoproterozoic Glaciations. Geological
624 Society 36, London, pp. 51-66.

625 Hansell, D. A., 2013. Recalcitrant Dissolved Organic Carbon Fractions. Annual
626 Review of Marine Science 5, 421-445.
627 Hoffman, P.F., 2005. On Cryogenian (Neoproterozoic) ice-sheet dynamics and the
628 limitations of the glacial sedimentary record. South African Journal of Geology
629 108, 557-577.
630 Hoffman, P.F., 2011. Strange bedfellows: glacial diamictite and cap carbonate from
631 the Marinoan (635 Ma) glaciation in Namibia. Sedimentology 58, 57-119.
632 Hoffman, P.F., Schrag, D.P., 2002. The snowball Earth hypothesis: testing the limits
633 of global change. Terra Nova 14, 129-155.
634 Holland, H.D., 1999. When did the Earth's atmosphere become oxic? A Reply. The
635 Geochemical News 100, 20-22.
636 Holland, H.D., 2006. The oxygenation of the atmosphere and oceans. Philosophical
637 Transactions of the Royal Society B 361, 903-915.
638 Hollander, D.J., Smith, M.A., 2001. Microbially mediated carbon cycling as a
639 control on the $\delta^{13}C$ of sedimentary carbon in eutrophic Lake Mendota (USA): new
640 models for interpreting isotopic excursions in the sedimentary record. Geochimica
641 et Cosmochimica Acta 65, 4321–4337.
642 Jiang, G., Sohl, L.E., Christie-Blick, N., 2003. Neoproterozoic stratigraphic
643 comparison of the Lesser Himalaya (India) and Yangtze Block (South China):
644 paleogeographic implications. Geology 31, 917-920.
645 Jiang, G., Shi, X., Zhang, S., et al., 2011. Stratigraphy and paleography of the
646 Ediacaran Doushantuo Formation (ca. 635-551 Ma) in South China. Gondwana

647 Research 19, 831-849.
648 Jiang, G., Wang, X., Shi, X., et al., 2012. The origin of decoupled carbonate and
649 organic carbon isotope signatures in the early Cambrian (ca. 542-520 Ma) Yangtze
650 platform. Earth and Planetary Science Letters 317-318, 96-110.
651 Jiang, G., Wang, X., Shi, X., et al., 2010. Organic carbon isotope constraints on the
652 dissolved organic carbon (DOC) reservoir at the Cryogenian-Ediacaran transition.
653 Earth and Planetary Science Letters 299, 159-168.
654 Jiao, N., Herndl, G.J., Hansell, D.A., et al., 2010. Microbial production of
655 recalcitrant dissolved organic matter: long-term carbon storage in the global ocean.
656 Nature reviews. Microbiology 8, 593–599
657 Johnston, D.T., Macdonald, F.A., Gill, B.C., et al., 2012. Uncovering the
658 Neoproterozoic carbon cycle. Nature 483, 320-323.
659 Kalinenko, V.V., 2001. Clay minerals in sediments of the Arctic Seas. Lithology and
660 Mineral Resources 36(4), 362-372.
661 Kump, L.R., Junium, C.J., Arthur, M.A., et al., 2011. Isotopic evidence of Massive
662 oxidation of organic matter following the Great oxidation event. Science 334,
663 1694-1696.
664 Lee, C., Love, G.D., Fischer, W.W., et al., 2015. Marine organic matter cycling
665 during the Ediacaran Shuram excursion. Geology 43(12), 1103-1106.
666 Li, C., Love, G.D., Lyons, T.W., et al., 2010. A stratified redox model for the
667 Ediacaran ocean. Science 328, 80-83.
668 Li, C., Love, G.D., Lyons, T.W., et al., 2012. Evidence for a redox stratified
669 Cryogenian marine basin, Datangpo Formation, South China. Earth and Planetary

670 Science Letters 331-332, 246-256.
671 Li, C., Cheng, M., Thomas, J.A., et al., 2015. A theoretical prediction of chemical
672 zonation in early oceans (>520Ma). Science China: Earth Sciences 58(11),
673 1901-1909.
674 Li, Z.X., Li, X.H., Kinny, P.D., et al., 1999. The breakup of Rodinia: did it start with
675 a mantle plume beneath South China?. Earth and Planetary Science Letters 173(3),
676 71-181.
677 Liu, P.J., Li, X.H., Chen, S.M. et al., 2015. New SIMS U-Pb zircon age and its
678 constraint on the beginning of the Nantuo glaciation. Chinese Science Bulletin 60:
679 958–963.
680 Liu, Y., Peltier, W.R., 2011. A carbon cycle coupled climate model of Neoproterozoic
681 glaciation: Explicit carbon cycle with stochastic perturbations. Journal of
682 Geophysical Research Atmospheres 116, D02125.
683 Liu, Y., Peltier, W.R., 2013. Sea level variations during snowball Earth formation: 1.
684 A preliminary analysis. Journal of Geophysical Research-Solid Earth 118,
685 4410-4424.
686 Lyons, T.W., Reinhard, C.T., Planavsky, N.J., 2014. The rise of oxygen in Earth's
687 early ocean and atmosphere. Nature 506, 307-315.
688 Macdonald, F.A., Schmitz, M.D., Crowley, J.L., et al., 2010. Calibrating the
689 cryogenian. Science 327, 1241-1243.
690 McFadden, K.A., Huang, J., Chu, X., et al., 2008. Pulsed oxidation and biological
691 evolution in the Ediacaran Doushantuo Formation. Proceedings of the National

692 Academy of Sciences of the United States of America 105 (9), 3197-3202.
693 Mckirdy, D.M., Burgess, J.M., Lemon, N.M., et al., 2001. A chemostratigraphic
694 overview of the late Cryogenian interglacial sequence in the Adelaide Fold-Thrust
695 Belt, South Australia. Precambrian Research 106(1-2): 149-186.
696 Rooney, A.D., Macdonald, F. A, Strauss, J. V, et al., 2014. Re-Os geochronology and
697 coupled Os-Sr isotope constraints on the Sturtian snowball Earth. Proceedings of
698 the National Academy of Sciences of the United States of America 111, 51–56.
699 Rooney, A.D., Strauss, J.V., Brandon, A.D., 2015. A Cryogenian chronology: Two
700 long-lasting synchronous Neoproterozoic glaciations. Geology 43(5), 459-462.
701 Rose, C.V., Swanson-Hysell, N.L., Husson, J.M., et al., 2012. Constraints on the
702 origin and relative timing of the Trezona $\delta^{13}C$ anomaly below the end-Cryogenian
703 glaciation. Earth and Planetary Science Letters 319-320, 241-250.
704 Rothman, D.H., Hayes, J.M., Summons, R.E., 2003. Dynamics of the
705 Neoproterozoic carbon cycle. Proceedings of the National Academy of Sciences of
706 the United States of America 100 (14), 8124–8129.
707 Schrag, D.P., Berner, R.A., Hoffman, P. F., et al., 2002. On the initiation of a
708 snowball Earth. Geochemistry, Geophysics, Geosystems 3(6), 1-21.
709 Schrag, D.P., Higgins, J.A., Macdonald, F.A., et al., 2013. Authigenic carbonate and
710 the history of the global carbon cycle. Science 339, 540-543.
711 Shen, Y., Zhang, T., Chu, X., et al., 2005. C-isotope stratification in a Neoproterozoic
712 postglacial ocean. Precambrican Research 137, 243-251.
713 Shields, G.A., Stille, P., Brasier, M., Atudorei, N.-V., 1997. Stratified oceans and

714 oxygenation of the late Precambrian. Terra Nova 9, 218–222.
715 Shields, G.A., Brasier, M.D., Stille, P., et al., 2002. Factors contributing to high $\delta^{13}C$
716 values in Cryogenian limestones of western Mongolia. Earth and Planetary Science
717 Letters 196, 99–111.
718 Smith, M.P., Harper, D.A., 2013. Causes of the Cambrian Explosion. Science 341,
719 1355-1356.
720 Sperling, E.,A., Wolock, C.J., Morgan, A.S., et al., 2015. Statistical analysis of iron
721 geochemical data suggests limited late Proterozoic oxygenation. Nature 523, 23,
722 451-454.
723 Squire, R.J., Campbell, I.H., Allen, C.M., et al., 2006. Did the Transgondwanan
724 Supermountain trigger the explosive radiation of animals on Earth. Earth and
725 Planetary Science Letters 250, 116-133.
726 Swanson-Hysell, N.L., Rose, C.V., Calmet, C.C., et al., 2010. Cryogenian Glaciation
727 and the Onset of Carbon-Isotope Decoupling. Science 30(328), 608-611.
728 Summons, R.E., Franzmann, P.D., Nichols, P.D., 1998. Carbon isotopic fractionation
729 associated with methylotrophic methanogenesis. Organic Geochemistry 28(7-8),
730 465-475.
731 Thiry, M., 2000. Palaeoclimatic interpretation of clay minerals in marine deposits: an
732 outlook from continental origin. Earth-Science Reviews 49, 201-221.
733 Wang, X., Jiang, G., Shi, X., et al., 2016. Paired carbonate and organic carbon
734 isotope variations of the Ediacaran Doushantuo Formation from an upper slope
735 section at Siduping, South China. Precambrian Research 273, 53-66.

736 Wu, C., Zhang, Z., Xiao, J., et al., 2016. Nanhuan manganese deposits within
737 restricted basins of the southeastern Yangtze Platform, China: Constraints from
738 geological and geochemical evidence. Ore Geology Reviews 75: 76-99.
739 Zhang, F., Zhu, X., Yan, B., et al., 2015. Oxygenation of a Cryogenian ocean
740 (Nanhua Basin, South China) revealed by pyrite Fe isotope compositions. Earth
741 and Planetary Science Letters 429, 11-19.
742 Zhang, Q., Chu, X., Bahlburg, H., et al., 2003. Stratigraphic architecture of the
743 Neoproterozoic glacial rocks in the 'Xiang-Qian-Gui' region of the central Yangtze
744 Block, South China. Progress in Natural Science 13(10), 783-787.
745 Zhang, S., Evans, D.A.D, Li, H., et al., 2013. Paleomagnetism of the late Cryogenian
746 Nantuo Formation and paleogeographic implications for the South China Block.
747 Journal of Asian Earth Sciences 72, 164-177.
748 Zhang, S., Jiang, G., Han, Y., 2008. The age of the Nantuo Formation and Nantuo
749 glaciation in South China. Terra Nova 20(4), 289-294.
750 Zhang, S., Jiang, G., Zhang, J., et al., 2005. U-Pb sensitive high-resolution ion
751 microprobe ages from the Doushantuo Formation in South China: constraints on
752 late Neoproterozoic glaciations. Geology 33(6), 473-476.
753 Zhang, X., Shu, D., Han, J., et al., 2014. Triggers for the Cambrian explosion:
754 Hypotheses and problems. Gondwana Research 25, 896-909.
755 Zhou, C., Tucker, R., Xiao, S., et al., 2004. New constraints on the ages of
756 Neoproterozoic glaciations in south China. Geology 32(5), 437-440.
757 Zhu, M., Zhang, J., Yang, A., et al., 2007. Integrated Ediacaran (Sinian)

chronostratigraphy of South China. Palaeogeography, Palaeoclimatology, Palaeoecology 254, 7-61.